# Transmission confocal laser scanning microscopy with a virtual pinhole based on nonlinear detection

**C. Yang and J. Mertz**

*Laboratoire de Neurophysiologie et Nouvelles Microscopies, Ecole Supérieure de Physique et Chimie Industrielles, Institut National de la Santé et de la Recherche Médicale EPI-0002, Centre National de la Recherche Scientifique FRE-2500, 10 rue Vauquelin, 75005 Paris, France*

Received September 17, 2002

We present a transmission-mode confocal laser scanning microscope system based on the use of second-harmonic generation (SHG) for signal detection. Our method exploits the quadratic intensity dependence of SHG to preferentially reveal unscattered signal light and reject out-of-focus scattered background. The SHG crystal acts as a virtual pinhole that remains self-aligned without the need for descanning. © 2003 Optical Society of America

*OCIS codes:* 180.1790, 170.6900, 190.4160.

Confocal laser scanning microscopy (CLSM) is based on the use of a pinhole in the detection path to provide three-dimensional image resolution and enhanced background rejection.[1,2] In the usual CLSM implementation, detected light is descanned such that the pinhole effectively tracks the position of the laser focus at the sample. One can readily accomplish such descanning in a reflection configuration by retracing the signal path through the laser scanning optics. In a transmission configuration, however, descanning is technically much more difficult and typically requires the use of a second synchronized scanning system[1] or of an elaborate beam path to redirect the transmitted light in the backward direction.[3,4] We present a simple technique for accomplishing self-aligned descanning in transmission CLSM based on signal conversion with a second-harmonic-generation (SHG) crystal.

In standard transmission CLSM, laser light transmitted through the sample is focused onto a pinhole of area $A_p$ before detection. If the transmitted light has power $P$ and is distributed over a characteristic area $A$ at the pinhole plane, the detected power scales as $PA_p/A$ (assuming that $A_p < A$). In our method the pinhole is replaced by a thin nonlinear crystal, and only SHG is detected. Because SHG scales quadratically with incident intensity, the resultant signal scales approximately as $P^2/A$. In both cases the detected signal scales inversely with $A$, implying that out-of-focus light at the aperture (or crystal) plane is rejected. A distinct advantage of using a SHG crystal instead of a pinhole is that the crystal has a large area, allowing it to act as an aperture even when the transmitted signal light is not descanned. That is, the crystal may be thought of as a self-aligned virtual pinhole.

We demonstrate the principle described above with the experimental setup shown in Fig. 1. We use a mode-locked Ti:sapphire laser (Spectra-Physics) to generate laser pulses with 860-nm wavelength, ~100-fs duration, and 82-MHz repetition rate that are focused into a target sample with a 60×, 0.9-N.A. water-immersion objective (Olympus; focal waist, $w_0 = 0.5\ \mu$m). The transmitted light is collected with an identical objective and refocused onto a type I 200-$\mu$m-thick lithium triborate crystal (Castech). The total magnification factor, $M$, from the sample to the crystal is approximately 30, leading to a confocal parameter at the crystal of ~800 $\mu$m (i.e., the crystal is thin relative to this confocal parameter). The laser power incident upon the sample, $P_0$, is typically 10 mW. The laser beam is raster scanned in the $x$–$y$ direction with galvanometer-mounted mirrors, and the sample is scanned in the $z$ direction with a motorized translation stage.

To begin, we consider the signal obtained from a single isolated scatterer, a latex bead, which we scan in the $z$ direction, yielding the axial point-spread function of our apparatus ($z = 0$ denotes the focal plane). We observe first that, in our imaging configuration, the phase of the scattered light at the crystal plane is approximately in quadrature with that of the unscattered light, independently of bead position $z$. This result is a consequence of the cumulative Guoy shifts[5] incurred by both the scattered and the unscattered beams before they reach the crystal plane (when $z \gg w_0{}^2/\lambda$ the scattered beam incurs no net Guoy shift). To a good approximation, the total intensity incident at the crystal plane is then simply given by the sum of the respective unscattered and scattered intensities:

$$I(r,z) = P_0[(1-\epsilon_z)W_0(r) + \epsilon_z \eta W_S(r,z)], \qquad (1)$$

where $r$ is the radius from the optical axis at the crystal plane (we assume cylindrical symmetry), $\epsilon_z P_0$ is the

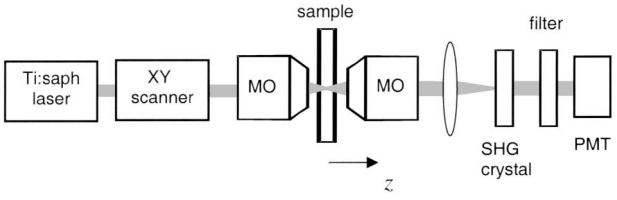


Fig. 1. Experimental layout: MO's, microscope objectives; PMT, photomultiplier tube. The filter transmits only SHG light.

0146-9592/03/040224-03$15.00/0 

total power scattered by the bead, $\eta$ is the fraction of this power accepted by the microscope exit pupil (defined here by the collection objective), and $W_{0,S}(r)$ are flux densities normalized such that $2\pi \int W_{0,S}(r) r \mathrm{d}r = 1$. These functions allow us to define the characteristic areas $A_{IJ} = [2\pi \int W_I(r) W_J(r) r \mathrm{d}r]^{-1}$. Inasmuch as the SHG produced by the crystal is proportional to $\int I^2(r) r \mathrm{d}r$, we conclude that

$$\frac{\mathrm{SHG}}{\mathrm{SHG}_0} = (1-\epsilon_z)^2 + 2\epsilon_z(1-\epsilon_z)\eta\,\frac{A_{00}}{A_{0S}} + {\epsilon_z}^2\eta^2\,\frac{A_{00}}{A_{SS}}. \tag{2}$$

Several comments are in order. First, $A_{00}/A_{0S}$ and $A_{00}/A_{SS}$ are smaller than 1 because $W_0(r)$ corresponds to a diffraction-limited intensity profile. Second, it is apparent that, as far as scattered light is concerned, $A_{00}/A_{0S}$ and $A_{00}/A_{SS}$ act as apertures, similarly to the microscope exit pupil. The smaller the values of $A_{00}/A_{0S}$ and $A_{00}/A_{SS}$, both of which depend on $z$, the less the scattered light contributes to the SHG signal (i.e., the more the scattered light is rejected). Finally, for purposes of comparison, we note that if the SHG crystal were removed and the power directly detected and squared, the expression for $P^2/{P_0}^2$ would be given by Eq. (2) with the replacements $A_{00}/A_{0S} \to 1$ and $A_{00}/A_{SS} \to 1$. In other words, direct detection of power provides no rejection of scattered light beyond that of the exit pupil. Figure 2 illustrates $\mathrm{SHG}/\mathrm{SHG}_0$ and $P^2/{P_0}^2$ for a Z scan of a 530-nm-diameter bead. In both cases, the presence of the bead is recognized as a reduction in unscattered laser power [first term in Eq. (2)]. This reduction is undermined by the concurrent detection of forward-directed scattered power that is transmitted through the exit pupil, which we refer to as background [second and third terms in Eq. (2)]. Because background rejection is more efficient with SHG than with direct detection, our method leads to a more highly contrasted bead signal.

We can roughly estimate the parameters in Eq. (2) in a paraxial approximation by assuming that $W_0(r)$ and $W_S(r, z)$ are Gaussian in profile, leading to $A_{00} \approx M^2\pi {w_0}^2$, $A_{SS} \approx M^2\pi {w_S}^2[1 + (\lambda z/\pi {w_S}^2)^2]$, and $A_{0S} = (A_{00} + A_{SS})/2$, where $w_S$ is the effective bead radius as it appears through the microscope's exit pupil. Scattering parameter $\epsilon_z$ depends on $z$ because it depends on the laser intensity incident upon the bead. We denote $\sigma$ as the bead-scattering cross section; then $\epsilon_z \approx \sigma/U_z$, where $U_z = {}^1\!/_2\,\pi {w_0}^2[1 + (\lambda z/\pi {w_0}^2)^2]$ is the effective area of the laser beam at axial position $z$. Pupil transmission $\eta$, however, is approximately independent of $z$ for small values of $z$. The following estimates are derived from Mie theory[6]: $\sigma \approx \pi \times (0.15\ \mu\mathrm{m})^2$, $w_S \approx 0.83\ \mu\mathrm{m}$, and $\eta \approx 0.75$. As is evident from a comparison with experimental data, our Gaussian approximation is overly simplistic and cannot account for the observed ringing in the SHG trace, presumably caused by pupil apodization. Nevertheless, it illustrates a salient principle of our microscopy technique, namely, that $A_{00}/A_{0S}$ and $A_{00}/A_{SS}$ are smaller than 1, leading here to an improvement in signal contrast with SHG detection.

To demonstrate that virtual pinhole microscopy with SHG detection also leads to improved out-of-focus background rejection, we acquire a $z$ stack of $x$–$y$ scans of a slab of 1-$\mu$m latex beads suspended in 0.3% agarose (number concentration, $N = 0.0071\ \mu\mathrm{m}^{-3}$; slab thickness, $L = 170\ \mu\mathrm{m}$). Because $\epsilon_z$ fluctuates randomly for different $x$–$y$–$z$ positions in the slab, we write $\epsilon_z = \langle\epsilon_z\rangle + \delta\epsilon_z$, where the angle brackets refer to the average over an ensemble of $x$–$y$ scans. If the scattering beads are randomly distributed in the slab and $\delta z$ is chosen large enough that $\epsilon_z$ and $\epsilon_{z+\delta z}$ are uncorrelated, then $\langle\epsilon_z\rangle \approx N\sigma\delta z$ and $\langle\delta{\epsilon_z}^2\rangle \approx N\sigma^2\delta z/U_z$. Though these last expressions require that $\sigma \ll U_z$, meaning that their validity breaks down somewhat in the immediate vicinity of the focal plane, we infer that $\langle\epsilon_z\rangle$, $\langle\delta{\epsilon_z}^2\rangle \ll 1$ throughout most of the sample. Equation (2) then leads to the approximation

$$\frac{\langle\mathrm{SHG}\rangle}{\mathrm{SHG}_0} \approx \prod_{z=z_{\mathrm{slab}}-L/2}^{z_{\mathrm{slab}}+L/2}\left[1 - 2\langle\epsilon_z\rangle\left(1 - \eta_z\,\frac{A_{00}}{A_{0S}}\right) + \langle\delta{\epsilon_z}^2\rangle\left(1 - 2\eta_z\,\frac{A_{00}}{A_{0S}} + {\eta_z}^2\,\frac{A_{00}}{A_{SS}}\right)\right], \tag{3}$$

where $z_{\mathrm{slab}}$ is the axial location of the slab center and $\eta_z$ is no longer assumed to be constant because $|z|$ can be large. Expression (3) is readily evaluated with the substitution $\prod_z[1 - f(z)\delta z] \approx \exp[-\int_z f(z)\delta z]$, yielding

$$\frac{\langle\mathrm{SHG}\rangle}{\mathrm{SHG}_0} \approx \exp\left[-2N\sigma\int_{z_{\mathrm{slab}}-L/2}^{z_{\mathrm{slab}}+L/2}\left(1 - \eta_z\,\frac{A_{00}}{A_{0S}} - \frac{\sigma}{2U_z}\right)\delta z\right], \tag{4}$$

where only the dominant terms have been kept. Relation (4) can be analytically expressed when the Gaussian approximation is used. Again for comparison, we note that, in the case of direct detection,

$$\frac{\langle P\rangle^2}{{P_0}^2} \approx \exp\left[-2N\sigma\int_{z_{\mathrm{slab}}-L/2}^{z_{\mathrm{slab}}+L/2}(1 - \eta_z)\delta z\right]. \tag{5}$$

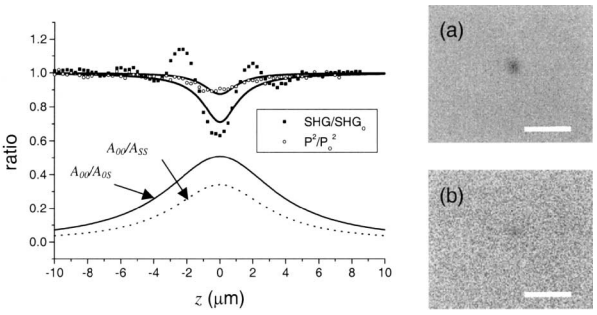


Fig. 2. Measured $\langle\mathrm{SHG}\rangle/\mathrm{SHG}_0$ and $\langle P\rangle^2/P_0^2$ for a Z scan of a 530-nm latex bead (averaged over five scans). Traces are derived from a Gaussian approximation model. (a) Nonaveraged SHG and (b) direct $P^2$ $x$–$y$ scans of the bead. Scale bars, 5 $\mu$m.

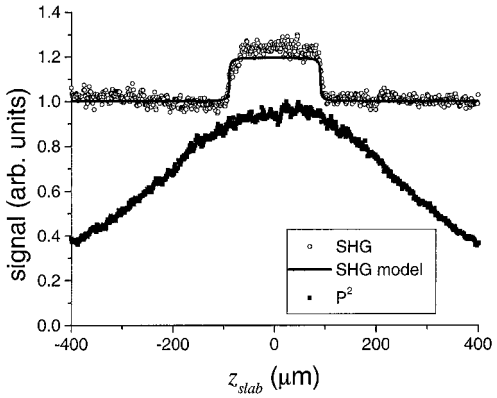


Fig. 3. Measured ⟨SHG⟩ and $\langle P\rangle^2$ for a Z scan of a 170-$\mu$m-thick agarose slab of 1-$\mu$m latex beads, and a theoretical trace derived from a Gaussian approximation, normalized to arbitrary units.

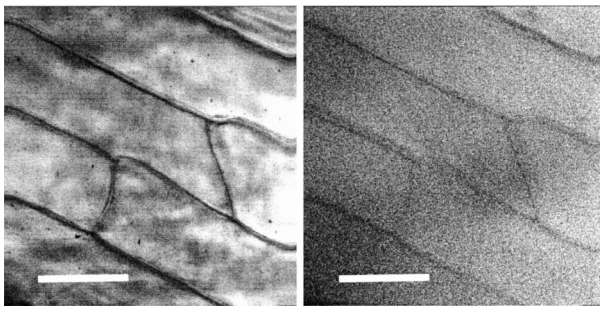

Fig. 4. $x-y$ images of an onion slice beneath a 200-$\mu$m agarose slab of 1-$\mu$m latex beads obtained left, by SHG detection and right, by direct $P^2$ detection. Scale bars, 100 $\mu$m.

In particular, we observe that SHG detection is sensitive to $\delta\epsilon_z{}^2$, whereas direct detection is not.

Figure 3 illustrates both SHG and direct detection signals, averaged over $x-y$, for various values of $z_{\mathrm{slab}}$. The qualitative difference in the traces is striking. The large but gradual increase in $\langle P\rangle^2$ as the slab approaches the focal plane indicates that a significant fraction of the transmitted power consists of out-of-focus scattered light. This is expected from the fact that the scattering is mostly forward directed ($\eta_z \approx 0.9$ near the focal plane). As is manifest from Fig. 3, the slab displacement must be quite large ($|z_{\mathrm{slab}}| > 400$ $\mu$m) before scattered light is significantly rejected by the exit pupil. In contrast, out-of-focus scattered light is much more efficiently rejected when SHG detection is used because $A_{00}/A_{0S}$ tends toward zero for relatively small displacements from the focal plane (see Fig. 2). When complete rejection is achieved, only unscattered light produces signal, and ⟨SHG⟩ and $\langle P\rangle^2$ are both proportional to $\exp(-2N\sigma L)$, which is $z$ independent. The apparent plateau in the SHG trace stems from the fact that $A_{00}/A_{0S}$ and $\delta\epsilon_z{}^2$ are nonnegligible only when the slab spans the focal plane. This plateau clearly identifies the slab boundaries, demonstrating the advantage of improved out-of-focus background rejection with SHG detection.

Finally, for purposes of illustration, we use our virtual pinhole technique to image an onion slice submerged under a 200-$\mu$m suspension of 1-$\mu$m latex beads (number concentration, $N = 0.0048$ $\mu\mathrm{m}^{-3}$). The ⟨SHG⟩ image and the corresponding $\langle P\rangle^2$ image are shown in Fig. 4. The former exhibits both a marked improvement in signal contrast and suppression of speckle noise that presumably is caused by scattered background.

In conclusion, we have demonstrated a new implementation of transmitted light confocal laser-scanning microscopy in which a second-harmonic-generation crystal serves as a self-aligned virtual pinhole. Because the SHG signal scales inversely with the area of the distribution of incident light, it preferentially reveals unscattered (focused) rather than scattered (diffuse) transmitted power. We emphasize that our technique works well, provided that an adequate supply of unscattered light survives transmission through the sample. The fact that unscattered power decays exponentially with sample thickness imposes limits on the technique's applicability. In particular, for thick samples the SHG signal from unscattered light can easily be dominated by the SHG from scattered background, despite the suppression of the latter by the virtual pinhole effect. We have empirically observed, with samples that comprise 1-$\mu$m beads, that our technique is effective up to sample thicknesses of roughly $3/N\sigma$ (i.e., three scattering lengths).

A notable advantage of our technique lies in its ease of implementation, particularly in combination with standard two-photon-excited microscopy,[7] which can be operated simultaneously. Finally, we note that our technique is not limited to signal conversion with a SHG crystal. Other techniques that involve, for example, two-photon-excited fluorophores or wide-bandgap semiconductors could achieve similar virtual pinhole effects.

We thank L. Moreaux for initial work on this project. C. Yang is grateful to the Institut National de la Santé et de la Recherche Médicale (France) for a postdoctoral fellowship (*Poste Vert)* and to the Agency for Science, Technology and Research (Singapore) for financial support. J. Mertz's e-mail address is jerome.mertz@espci.fr.

## References

1. M. Minsky, "Microscopy Apparatus," U.S. patent 3,013,467 (November 7, 1957).
2. T. Wilson and C. Sheppard, *Theory and Practice of Scanning Optical Microscopy* (Academic, London, 1984).
3. A. E. Dixon, S. Damaskinos, and M. R. Atkinson, Nature **351,** 551 (1991).
4. G. J. Brakenhoff, J. Microsc. **117,** 233 (1979).
5. M. Born and E. Wolf, *Principles of Optics*, 7th ed. (Cambridge U. Press, Cambridge, 1999).
6. C. Bohren and D. Huffman, *Absorption and Scattering of Light by Small Particles* (Wiley-Interscience, New York, 1983).
7. W. Denk, J. H. Strickler, and W. W. Webb, Science **248,** 73 (1990).